TROPICAL CYCLONES

Kerry Emanuel

Program in Atmospheres, Oceans, and Climate, Massachusetts Institute of Technology, Cambridge, Massachusetts 02139; email: emanuel@texmex.mit.edu

■ **Abstract**   Tropical cyclones encompass virtually every subdiscipline of geophysical fluid dynamics, including cumulus convection, boundary layers, thermodynamic cycles, surface wave dynamics, upper ocean wind-driven circulations, barotropic instability, Rossby waves, and air-sea interaction. After briefly reviewing what is known about the structure, behavior, and climatology of these fascinating storms, the author provides an overview of their physics, focusing on the unique and poorly understood nature of the air-sea interface, and discusses several of the most interesting avenues of ongoing research.

1. INTRODUCTION

Tropical cyclones, also popularly known as hurricanes or typhoons, are among the most spectacular and deadly geophysical phenomena. Both the most lethal and the most expensive natural disasters in U.S. history were tropical cyclones: The Galveston Hurricane of 1900 killed nearly 8000 people, and Hurricane Andrew of 1992 did more than $35 billion in damage. Globally, tropical cyclones rank with floods as the most lethal geophysical hazards. A single storm in Bangladesh in 1970 killed nearly half a million people. In spite of their importance and the publicity they receive, the physics of tropical cyclones are not well known outside a small group of specialists. The main purpose of this review is to provide a straightforward exposition of the physics of tropical cyclones, so far as they are understood today, and to expose a larger audience to some of the more exciting areas of ongoing research.

A brief overview of the climatology of tropical cyclones, their behavior, and their structure is provided in the following section. The physics of mature storms, focusing on energy sources and sinks, are discussed in Section 3, where it is made clear that storm intensity depends sensitively on the physical nature of the air-sea interface. The problems of the physics of the air-sea transfer at very high wind speeds, when the air is filled with sea spray, are described in Section 4, which also provides a summary of ongoing research on this issue. Vertical mixing of the upper ocean and its strong negative feedback on storm intensity are the subjects of Section 5.

The physics of tropical cyclone movement are reviewed in Section 6. The pressing problem of tropical cyclogenesis, about which comparatively little is understood, is described in Section 7, and the findings of some recent field experiments are presented. In recent years, there has been much progress in understanding the sub-storm structure of tropical cyclones, including the phenomenon of concentric eyewall cycles and spiral rainbands; this subject is reviewed in Section 8. Finally, the effect of climate change on tropical cyclone activity and the possible role of tropical cyclones in global climate are described in Section 9.

2. STORM SURVEILLANCE, BEHAVIOR, AND STRUCTURE

2.1 Definitions

Technically, a tropical cyclone is a cyclone that originates over tropical oceans and is driven principally by heat transfer from the ocean. Mostly for the purpose of providing useful warnings, tropical cyclones are categorized according to their maximum wind speed, defined as the maximum speed of the wind at an altitude of 10 m, averaged over 10 min (except in the United States, where a 1 min average is conventional). Tropical cyclones in their formative stage, with maximum winds of $17 \, ms^{-1}$ or less, are known as tropical depressions; when their wind speeds are in the range of 18 to $32 \, ms^{-1}$, inclusive, they are called tropical storms, whereas tropical cyclones with maximum winds of $33 \, ms^{-1}$ or greater are called hurricanes in the western North Atlantic and eastern North Pacific regions, typhoons in the western North Pacific, and severe tropical cyclones elsewhere.

2.2 Detection and Surveillance

Up until World War II, detection of tropical cyclones relied largely on reports from coastal stations, islands, and ships at sea. During this time, it is likely that many storms escaped detection entirely, and many others were observed only once or a few times during the course of their lives. This was particularly true in untraveled stretches of ocean and for storms that never made landfall. For example, very few storms were detected in the eastern North Pacific region where there is little shipping and storms almost never make landfall (see Figure 1).

The war brought about several major changes. During the war itself, military aircraft operating from Pacific island stations and aircraft carriers were tasked with finding tropical cyclones that could pose a danger to naval operations. These aircraft did not penetrate the interiors of strong storms until July 27, 1943, when an AT-6 trainer was flown into the eye of a Gulf of Mexico hurricane. This marked the beginning of tropical cyclone reconnaissance, which became routine by the late 1940s. At about the same time, the very first radar images (Wexler 1947) of tropical cyclones revealed the structure of precipitation, showing for the first time an unambiguous depiction of the eye and spiral rainbands and allowing detection of storms that were up to several hundred kilometers offshore.
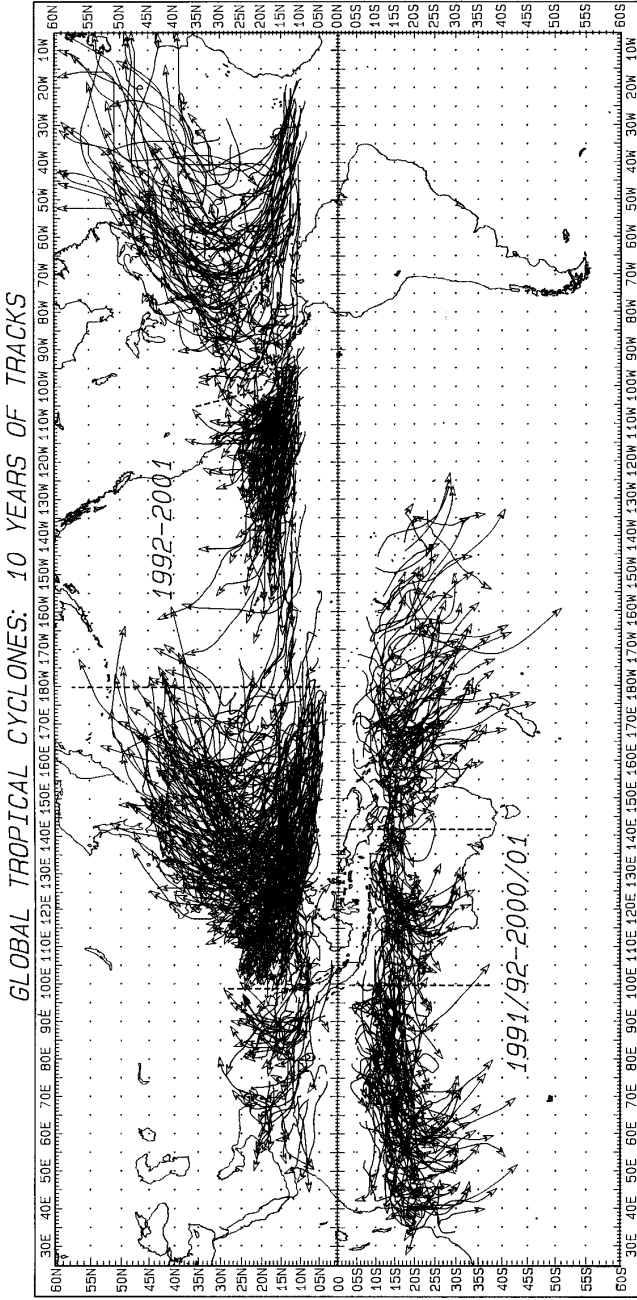
Figure 1 Tracks of tropical cyclones with wind speeds of at least 17 ms^{-1} for the period 1992–2001. Courtesy of Dr. Charles Neumann (Neumann 1993).

Although aircraft reconnaissance of Atlantic storms became routine, early methods of estimating wind speed were crude, and not until Doppler radar was used to estimate the ground speed of aircraft in the late 1950s were reliable estimates of wind speeds made.

A great step forward came in 1960, when the first image of a tropical cyclone was transmitted from a polar orbiting satellite. By the 1970s, virtually all tropical cyclones (with the possible exception of some of the elusive, so-called midget storms) were recorded by satellite observations. Satellites can virtually pinpoint the location of any tropical storm with a well-defined eye, and pattern-recognition techniques, as well as infrared radiance measurements, are brought to bear to estimate storm intensity using satellite-based measurements. There is some controversy concerning the accuracy of satellite-based wind estimates, but today they are the basis for most such estimates, except in the case of some Atlantic storms that are still surveyed by aircraft.

2.3 Climatology

Roughly 80 tropical cyclones develop globally each year. For reasons discussed in Section 2, tropical cyclones generally develop over ocean water whose surface temperature exceeds $26°$ C, but they often move out of these regions into higher latitudes. They always develop from pre-existing atmospheric disturbances, especially waves of 1000–3000 km in scale, as is discussed in Section 7. Figure 1 shows, for a ten-year period, the tracks of tropical cyclones with maximum winds in excess of $17 \, \text{ms}^{-1}$. Activity falls into three fairly well-defined belts. Tropical cyclones seldom form equatorward of $5°$ latitude; the record lowest latitude appears to be $1.6°$N, in the case of a typhoon that occurred in the Indonesian region around Christmas of 2001. (Tropical cyclones must form in a region where the absolute vorticity of the air flow has a nonzero value.) There has only been one documented tropical cyclone in the South Atlantic basin and it was quite weak. Once developed, the storms generally move westward and slightly poleward at speeds in the range of $2–10 \, \text{ms}^{-1}$. They usually quickly dissipate when they move over land or cold water; they sometimes dissipate over warm water owing to unfavorable interactions with other atmospheric wind systems. If they survive long enough, or form at a relatively high latitude, they often recurve poleward and eastward and accelerate as they are entrained into the strong west-to-east winds characteristic of the extratropical middle and upper troposphere (2–10 km altitude). Rapid poleward movement allows tropical cyclones to affect extratropical locations with severe winds and rains before the storms have had much time to dissipate, and interaction with extratropical disturbances can lead to slower decay or even to a brief period of re-intensification. Note in Figure 1 that the greatest poleward displacements are achieved by North Atlantic storms.

Although there are many possible measures of the intensity of tropical cyclones, it is customary to use maximum wind speed (see Subsection 2.1 above) or central surface pressure as measures. There are now enough measurements of tropical

cyclone wind speeds, since such estimates became accurate, to make some elementary statistical analyses of intensity. The author (Emanuel 2000) calculated cumulative frequency distributions of the wind speeds in North Atlantic and western North Pacific tropical cyclones. The peak winds reached during the storms, normalized by their theoretical maximum values (see Section 3), tend to fall into one of two linear cumulative distributions depending on whether the storm does or does not reach hurricane intensity, as shown in Figure 2. This means that a randomly chosen tropical cyclone has the same probability of reaching any given intensity up to marginal hurricane intensity, and another (but constant) probability of reaching any intensity between marginal hurricane intensity and the maximum theoretical intensity at that time and place.

In dimensional terms, maximum sustained winds in tropical cyclones may be as large as 85 ms^{-1}, as recorded in Typhoon Tip in the western North Pacific in October 1979.

Tropical cyclones are, for the most part, creatures of the summer and early autumn. In the North Atlantic region, they develop mostly during the months of June through November, reaching peak activity in September, whereas over the
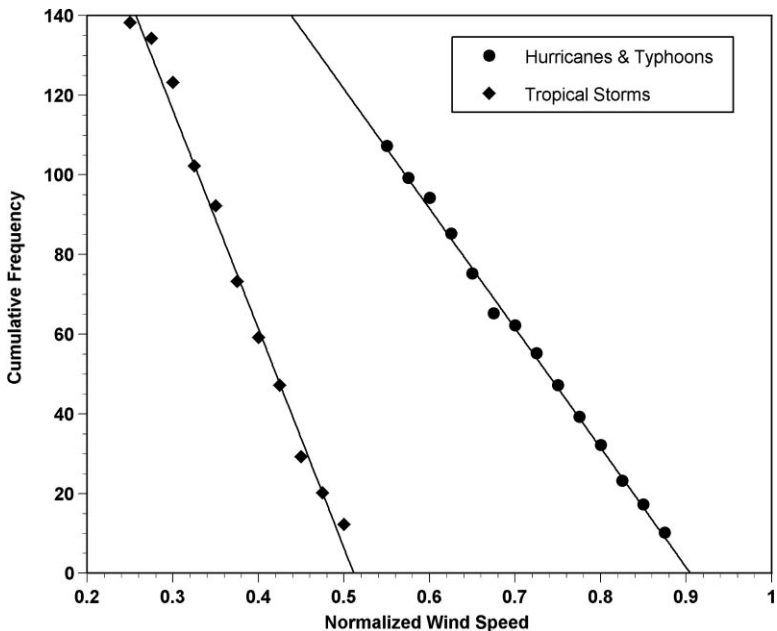

Figure 2   Total number of tropical cyclones with normalized wind speeds exceeding the value on the abscissa, from 1957 to 1999 in the North Atlantic and from 1970 to 1999 in the western North Pacific. The wind speeds have been normalized by the theoretical maximum wind speed calculated from climatological data using Equation 8. From Emanuel (2000).

eastern North Pacific, peak activity occurs in July and August. In the tropical western North Pacific belt, storms also reach peak activity in late summer, but have been observed at all times of the year. (A pair of December storms wreaked havoc on Admiral Halsey's U.S. Pacific fleet in 1944.) The South Pacific and South Indian Ocean belt is active during the warmer months in the Southern Hemisphere, from October through June. A more complete description of the climatology of tropical cyclones may be found in Pielke (1990).

Vortices that strongly resemble tropical cyclones occasionally form well outside the tropics, including in the Mediterranean (see, e.g., Reale & Atlas 2001) and sometimes at very high latitudes, where they are referred to as polar lows. Although this phenomenon may encompass a broad class of physical processes, some of these events appear to be physically isomorphic to tropical cyclones (Emanuel & Rotunno 1989). Most occur during the colder months, especially in autumn and winter. A survey of polar low climatology and physics is provided by Twitchell et al. (1989).

2.4 Structure of Mature Storms

Most of what we know about the structure of tropical cyclones has been obtained from detailed measurements made directly by reconnaissance aircraft; from small instrument packages (dropwindsondes) deployed from them; and from ground-based and airborne radar, including Doppler radar capable of measuring airflow. In recent years, this has been supplemented by measurements from satellites and from highly detailed numerical simulations of storms. All of these measurements paint a picture of a tropical cyclone as an approximately axisymmetric vortex, but with interesting and perhaps important asymmetries that are discussed in Section 8. Detailed composite analyses of tropical cyclone structure based on aircraft data can be found in Frank (1977a,b), Jorgensen (1984), and Weatherford & Gray (1988), and Marks & Houze (1987) provide a nice example of analysis of kinematic structure made possible by airborne Doppler radar. The invention of lightning detection networks has allowed for a detailed mapping of lightning in hurricanes near land, showing interesting relationships to the structure and evolution of the storms (Molinari et al. 1994).

A composite view of a mature tropical cyclone is provided in Figure 3, showing a cutaway view in which the cloud structure of a particular storm (Hurricane Fran of 1996) as seen by satellite is shown at the top, whereas the left-hand cross-section shows the distribution of the azimuthal wind component in another storm (Hurricane Inez of 1966) and the right-hand cross-section shows the distribution of the vertical velocity component in a numerical simulation of a hurricane.

Winds throughout most of the volume occupied by tropical cyclones flow cyclonically (in the same sense as the local vertical component of the earth's rotation), but near the top of the storm, the sense of rotation reverses and is anticyclonic,

except perhaps very near the storm center. Winds increase rapidly outward from the center, reaching maximum strength 10–100 km from the center, and then fall off more gradually with radius, roughly following an $r^{-1/2}$ decay law near the radius of maximum winds, but falling off faster at larger radii. At radii of between 100 and 1000 km, wind speeds become indistinguishable from those normally found in the tropical atmosphere. The maximum winds occur very near the surface and decay slowly upward, finally reversing direction near the storm top. (Although the flow through most of the troposphere may be approximately axisymmetric, the flow near the storm top is rarely so, usually being concentrated in one or more "outflow jets" that curve anticyclonically out from the storm core.) Translation of the storm as a whole leads to an asymmetry in the ground-relative wind field. To a reasonable approximation, the ground-relative winds are just the vector sum of the storm-relative wind velocities and the translation velocity.

The right-hand cutaway in Figure 3 shows a typical distribution of vertical velocity, in this case derived from a simple numerical model.[1] Maximum upflow occurs in the eyewall, a ring of very deep convective cloud extending from the outer edge of the eye outward another 20–50 km. The radius of maximum winds can usually be found in this region. Maximum ascent velocities are around 5–10 ms^{-1} and are usually found in the upper troposphere (Jorgensen et al. 1985). The actual upward flow of mass is carried by tall cumulonimbus clouds that, in weaker storms, have a cellular structure and characteristic dimensions of 10^2 km^2, but in intense storms, the clouds may themselves form a nearly axisymmetric ring. As discussed in Section 8, there may be two or even three eyewalls present at any given time, evolving through a characteristic cycle in which the outer eyewalls contract inward and replace dissipating inner eyewalls.

Well-developed tropical cyclones usually have eyes, defined as nearly cloud-free regions inside the eyewall. (An eye can be seen in the center of Figure 3.) Eyes are usually found in storms with maximum winds of hurricane strength or greater, although some fairly intense storms lack clearly defined eyes and weaker storms occasionally exhibit them. Air is slowly subsiding in the eyes, usually at velocities of 5–10 cms^{-1}. Air can subside somewhat more rapidly during rapid intensification of the storm, however. Outside the eyewall, air is also, on average, descending at a few cms^{-1}, but this descent is usually interrupted by spiral bands of cumulonimbus clouds, where air may be ascending at a few ms^{-1} (see Section 8).

Figure 4 shows a second cross-section through a hurricane, using output from the simple model referred to above. In the left half, the shading shows the difference between the temperature at any point and the temperature in the distant environment at the same altitude. This shows the dramatically hot core of the storm at higher altitudes; in this case, approximately 8°C warmer than the environment, though

---

[1]This can be run in a minute or less on a PC or workstation and can be obtained from the author at http://wind.mit.edu/~emanuel/modelftp.html.

much higher temperatures have been measured. The colored contours show the radial component of motion; the light contours at low levels show inflow, reaching peak speeds of approximately 10 ms^{-1}, and the darker colors at high levels show outflow, which may reach speeds of several tens of ms^{-1}. Note, however, that above the outflow there is another layer of very weak inflow descending into the outer edge of the eye.

In discussing the physics of tropical cyclones, it is helpful to refer to the distributions of two important conserved variables, as shown in the right half of Figure 4. The black contours show the distribution of absolute angular momentum, per unit mass, around the axis of the storm. This quantity is defined as

$$M = rV + \frac{1}{2} fr^2, \tag{1}$$

where r is the radius from the storm center; V is the tangential velocity; and f is the Coriolis parameter, which is just twice the projection of the earth's angular velocity vector onto the local vertical plane. The second term on the right of Equation 1 is the contribution of the earth's rotation to the angular momentum, whereas the first is the contribution from the rotating wind field. In the absence of frictional torque, M is conserved following axisymmetric displacements of fluid rings. In the absence of circulation, M is just a function of radius and contours of M are vertical. Note in Figure 4 that M decreases upward and inward and has very strong gradients in the eyewall. This is a consequence of the strong frontogenesis that occurs there, as described in the next section.

The shading on the right half of Figure 4 shows the distribution of a conserved thermodynamic variable, the specific entropy, with warmer colors denoting higher values. This quantity is conserved following reversible adiabatic displacements of air, even when water changes phase. It is a function of temperature, pressure, and water concentration and is defined approximately as

$$s \approx C_p \ln(T) - R_d \ln(p) + \frac{L_v q}{T} - q R_v \ln(\mathsf{H}), \tag{2}$$

where T is the absolute temperature, p the pressure, q the concentration of water vapor, and H the relative humidity. The thermodynamic parameters in Equation 2 are the heat capacity at constant pressure, C_p, the gas constants for dry air and water vapor, R_d and R_v, and the latent heat of vaporization, L_v.

As apparent in Figure 4, entropy increases inward, reaching maximum values in the eyewall. (The centers of tropical cyclones contain the highest values of entropy to be found anywhere at sea level.) At large radius, the entropy distribution resembles that of the unperturbed tropical environment, decreasing upward from the surface and reaching minimum values a few kilometers above the surface. Above this level, entropy increases with altitude, more rapidly in the stratosphere. Note also the strong radial entropy gradients in the eyewall.

These conserved variable distributions are useful for describing the physics and energetics of tropical cyclones, which are the subjects of the next section.

3. PHYSICS OF MATURE STORMS

3.1 Energetics

The basic source of energy for tropical cyclones is heat transfer from the ocean, as first recognized by Riehl (1950) and Kleinschmidt (1951). The mature tropical cyclone may be idealized as a steady, axisymmetric flow whose energy cycle is very similar to that of an ideal Carnot engine (Emanuel 1986). Referring to Figure 4, air begins to spiral in from the outer region (point *a* in Figure 4) toward the storm center. As can be seen in Figure 4, as it spirals in, it suffers a pressure drop and its entropy increases owing to both enthalpy transfer from the sea surface (mostly in the form of evaporation) and dissipation of kinetic energy in the atmospheric boundary layer (Bister & Emanuel 1998). At the same time, its angular momentum decreases because of frictional torque with the sea surface; this proves to be by far the most important sink of kinetic energy in the storm. Temperatures along this leg are nearly constant. At the eyewall (point *b* in Figure 4), the flow turns upward and closely follows surfaces of constant entropy and angular momentum as it ascends toward lower pressure; this leg is nearly adiabatic and free of frictional torque. In real storms, air flowing out near the storm top usually experiences strong exchanges with the environment, so the energy cycle is in fact open. But numerically simulated axisymmetric storms have closed cycles and behave very much like real storms, so we can idealize the cycle as closed. Air descends in the distant environment (symbolically between points *o* and *o'* in Figure 4), where the entropy acquired in the inflow leg is lost by electromagnetic radiation to space, and angular momentum is gained by mixing with the environment. This leg is nearly isothermal. (Some kinetic energy dissipation occurs here too, but unless the storm is very broad, this is minor.) The cycle is closed by an angular-momentum-conserving leg between points *o'* and *a*; although entropy is lost and gained during this leg, the implied irreversible entropy source is all produced by mixing of moist and dry air and little or none is available for kinetic energy production.

Thus, like the Carnot cycle, the energy cycle of a mature tropical cyclone is one of isothermal expansion (with addition of enthalpy), adiabatic expansion, isothermal compression, and adiabatic compression. But there is an important difference. The energy made available in the textbook Carnot cycle is used to do work on its environment. In tropical cyclones, on the other hand, work is used up in turbulent dissipation in the storm's atmospheric boundary layer,[2] where it is turned back into heat. Because this conversion is occurring at the highest temperature in the system, the hurricane recycles some of its waste heat back into the front end of the Carnot cycle (Bister & Emanuel 1998).

Both the heat input and the dissipation of kinetic energy in this cycle occur largely through air-sea transfer. The flux of momentum into the sea and the flux

---

[2]There is also kinetic energy dissipation in the upper ocean, but this is small in comparison.

of enthalpy from the sea are usually quantified using bulk formulae of the form

$$F_m = -C_D \rho |V| V \tag{3}$$

and

$$F_k = C_k \rho |V| (k_0^* - k), \tag{4}$$

where V is some near-surface wind speed, ρ is the air density, k is the specific enthalpy of air near the surface, and k_0^* is the enthalpy of air in contact with the ocean, assumed to be saturated with water vapor at ocean temperature. The dimensionless transfer coefficients of momentum and enthalpy are C_D and C_k. As discussed in Section 4, these coefficients depend on the sea state, but very little is known about their values at the very high wind speeds found in tropical cyclones. The vertically integrated dissipative heating of the atmospheric boundary layer can be modeled as

$$D = C_D \rho |V|^3 \tag{5}$$

(see Bister & Emanuel 1998). If we take the sea surface temperature to be T_s and the mean temperature of the cold source (between points o and o' in Figure 4) to be T_o, then the Carnot theorem tells us that the net production of mechanical energy in the cycle is

$$P = 2\pi \frac{T_s - T_o}{T_s} \int_a^b \left[C_k \rho |V| (k_0^* - k) + C_D \rho |V|^3 \right] r \, dr, \tag{6}$$

where the integral is taken over the first leg of the cycle. On the other hand, from Equation 5, the net energy dissipation is

$$D = 2\pi \int_a^b C_D \rho |V|^3 r \, dr. \tag{7}$$

If we assume that the integrals in Equations 6 and 7 are dominated by the values of their integrands near the radius of maximum wind speed, then equating Equations 6 and 7 gives an approximate expression for the maximum wind speed:

$$|V_{\max}|^2 \approx \frac{C_k}{C_D} \frac{T_s - T_0}{T_0} (k_0^* - k). \tag{8}$$

Although this derivation is approximate, the same expression results from an exact derivation, as shown by Bister & Emanuel (1998). Note that the middle term, which looks like a thermodynamic efficiency, has the outflow temperature rather than the inflow temperature in its denominator. This reflects the added contribution from dissipative heating. The last term is a measure of the thermodynamic disequilibrium that normally exists between the tropical ocean and atmosphere; this disequilibrium allows convective heat transfer to occur. In the unperturbed tropical climate, absorption of sunlight by the ocean is nearly balanced by convective heat transfer from the sea surface; because of the greenhouse effect, there is little

net longwave radiative flux from the sea. [There is a concern that anthropogenic increases in greenhouse gases may further reduce the net longwave emission from the tropical oceans, thereby increasing the thermodynamic disequilibrium and with it the intensity of tropical cyclones (Emanuel 1987).] The maximum wind speed also depends on the ratio of the transfer coefficients, but not on their individual values. Numerical simulations strongly confirm this predicted dependence on the transfer coefficients (Ooyama 1969, Rosenthal 1971, Emanuel 1995b) and also show that simulated storm intensities conform almost exactly to predictions made by Equation 8.

It is straightforward to calculate the maximum wind speed possible in tropical cyclones by applying Equation 8 to climatological atmospheric conditions and sea surface temperatures. This has been done by the author (Emanuel 1986), who presented global maps of maximum wind speed and minimum pressure.[3] It is this upper bound that has been used to normalize the maximum winds of observed tropical cyclones, whose cumulative frequency is plotted in Figure 2. In calculating the upper bound, the ratio of transfer coefficients was assumed to be unity for lack of better knowledge. Figure 2 suggests that in reality, this ratio may be slightly less than unity. Also, numerically simulated storms invariably spin up to the intensity given by Equation 8, whereas Figure 2 shows that few real storms achieve this limit. Reasons for this are discussed in Section 5.

Estimates of the kinetic energy dissipation made by applying Equation 7 to real storms show that the average tropical cyclone dissipates approximately 3×10^{12} W, equal to the rate of electrical power consumption in the United States in the year 2000. An exceptionally large and intense storm can dissipate an order of magnitude more power (Emanuel 1998).

3.2 Dynamics of Intensification and Eye Formation

Once the core of an incipient tropical cyclone becomes saturated with water through its depth, intensification proceeds through a feedback mechanism wherein increasing surface wind speeds produce increasing surface enthalpy flux (see Equation 4), while the increased heat transfer leads to increasing storm winds. Comparing Equation 4 with Equation 5 shows that the dissipation increases as the cube of the wind speed, whereas the heat transfer increases only as the first power of the wind speed, so that eventually the dissipation matches energy production and the storm achieves a quasi-steady state. A characteristic timescale over which the vortex evolves was shown by the author (Emanuel 1989) to be

$$\tau \approx \frac{H}{C_D V_{\max}}, \tag{9}$$

[3]These bounds are calculated every day by the Center for Ocean-Land-Atmosphere Studies and are available at http://grads.iges.org/pix/hurpot.html.

where H is an atmospheric scale height (~ 8 km), C_D is the surface drag coefficient, and $V_{\max}$ is given by Equation 8. For typical conditions, this is on the order of 15 h. This is also the time it takes air ascending in the eyewall to traverse the depth of the storm.

Using a coordinate system in which angular momentum is taken as the independent radial coordinate, the author (Emanuel 1997) was able to derive an equation for the intensification of the winds. Scaling time by Equation 9 and V by $V_{\max}$ as given by Equation 8, the resulting equation is approximately

$$\frac{\partial V^2}{\partial \tau} \simeq \alpha V(1 - V^2) + \beta(3V^2 - 1)M\frac{\partial V}{\partial M}, \tag{10}$$

where α and β are parameters that may vary with radius. The first term on the right side of Equation 10 accelerates the wind toward its maximum value, whereas the second term propagates the wind distribution relative to angular momentum surfaces in such a way that the peak wind migrates outward (in M space) for $V^2 < \frac{1}{3}$, and inward otherwise.

One curiosity of the intensification dynamics is the tendency toward frontogenesis, leading to strong gradients in the eyewall. Although there is little surface temperature gradient, there are strong gradients of entropy and angular momentum, as shown in Figure 4. Unlike classical atmospheric fronts, eyewall frontogenesis is actually driven by surface fluxes. The basic process can be understood with the aid of Figure 5. First, note in Figure 4 that in the eyewall, entropy and angular momentum surfaces are congruent. Thus, when entropy is plotted in angular momentum coordinates, as in Figure 5, surfaces of constant entropy are vertical. Second, note that the radial "velocity" in angular momentum coordinates is just $\frac{dM}{dt}$. The drag law given by Equation 3 implies that

$$\frac{dM}{dt} \sim -VM,$$

whereas hydrostatic and centripetal balance, coupled with the congruence of the entropy and angular momentum surfaces, can be used to show that

$$V^2 \sim -M\frac{ds}{dM}.$$

Thus, the velocity maximum occurs outside the maximum gradient of entropy, and the maximum radial velocity (in this coordinate) occurs outside the radius of maximum V. Referring to Figure 5, the transport of entropy by the radial motion increases the magnitude of the radial gradient of entropy. This in turn increases V, which increases $\frac{dM}{dt}$, etc. When $\frac{\partial V}{\partial M}$ reaches a finite positive value, mapping back into physical coordinates leads to a singularity with infinite vorticity: Frontal collapse has occurred (Emanuel 1997). This explains why the eyewalls of well-developed storms have such strong radial gradients of velocity and entropy.

The concentration of vertical vorticity into an annulus is very unstable and gives rise to a variety of eddies (Schubert et al. 1999) that transport vorticity into the eye of the storm, spinning it up. In the steady state, this spin-up is balanced by frictional
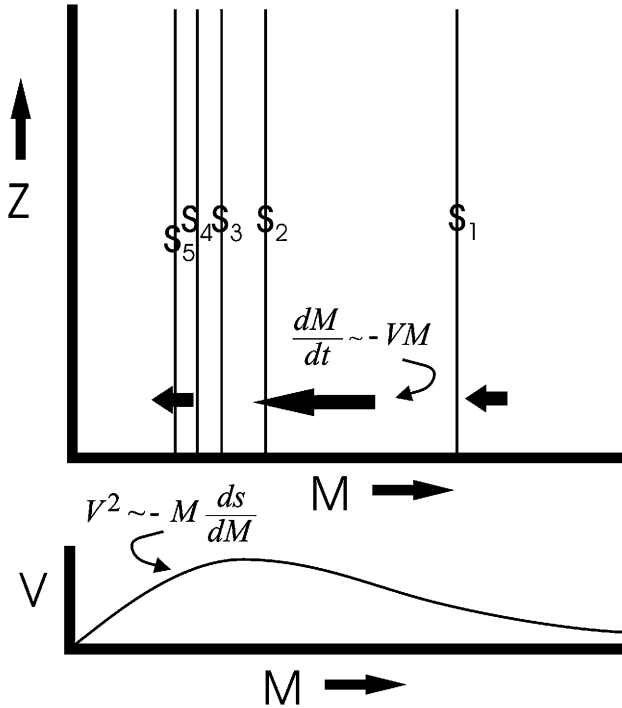
Figure 5   Sketch showing some aspects of eyewall dynamics. The radial coordinate is angular momentum rather than radius. The top panel shows the distribution with M and altitude of the entropy surfaces, and the black arrows show the radial wind in this coordinate space, $\frac{dM}{dt}$; this flow advects entropy in this coordinate. By the aerodynamic drag law, this is approximately equal to $-VM$. The lower panel shows the distribution of the tangential velocity V with M. Using centripetal and hydrostatic balance, it can be shown that $V^2 \sim -M\,{}^{ds}/{}_{dM}$. The flow tends to steepen the entropy gradient. See text for discussion.

torque with the underlying surface. To maintain centripetal and hydrostatic balance during the spin-up of the eye, the air within it must sink and warm by compression. Thus, the eye is a reverse heat engine, with mechanical energy supplied by the eyewall driving a heat pump that warms the eye itself. As the sinking air parcels warm, the saturation water vapor concentration increases rapidly, causing any condensed water to quickly evaporate, yielding the characteristic cloud-free eye. But very near the surface, frictionally induced inflow gives rise to upflow within a boundary layer that is 1–2-km thick; clouds often develop in this boundary layer.

3.3 Hypercanes

A closer look at the expression for maximum wind speed, Equation 8, reveals that it is an implicit expression. This is because the saturation enthalpy of the sea surface, k_0^*, is a function of pressure as well as temperature, increasing with

decreasing pressure. As winds increase, the surface pressure in the eyewall falls, increasing the value of k_0^*. This is a positive feedback that, under typical tropical conditions, contributes approximately 40% to the maximum wind speed. However, if the sea surface temperature is substantially greater, this feedback becomes strong enough that Equation 8 no longer has a solution (Emanuel 1988). This implies that the extra heat input from the ocean can no longer be balanced by surface-based dissipation, and any storm that might occur would be of a very different character. The author dubbed such storms hypercanes.

Emanuel et al. (1995) proposed that hypercanes might occur after the impact of a large comet or asteroid with the ocean. Numerical simulations show that seawater temperatures of at least 50°C are necessary to generate hypercanes. These simulations also suggest that hypercanes are relatively narrow, with eye dimensions of a few kilometers, and owing to extremely high specific entropy in the core, they can extend into the middle stratosphere. The authors proposed that such events might inject enough water into the middle stratosphere to destroy the ozone layer, thereby contributing to the mass extinctions that are thought to follow large asteroid impacts. The numerical code used in this work was designed for subsonic flows, but the simulated storms contained supersonic wind speeds. Thus, there is a need to revisit this problem using a numerical code capable of simulating flows with Mach numbers of order one.

4. AIR-SEA INTERACTION

Tropical cyclones are driven by enthalpy fluxes from the sea and limited mostly by surface drag, but there is little understanding of the wind-dependence of these fluxes at very high wind speeds. Direct measurements of the fluxes have been made at wind speeds as large as 25 ms^{-1}, but technical problems have thus far prevented reliable estimates at higher speeds. Within the range in which good measurements exist, the drag coefficient increases with wind speed, owing to the increasing roughness of the sea surface, but there is little evidence for a corresponding increase in the enthalpy exchange coefficient (Greeneart et al. 1987). Numerical experiments together with evaluation of Equation 8 make it clear that were these transfer functions continued to higher wind speeds, tropical cyclones could be of no more than marginal hurricane intensity. This suggests that another process, or processes, must become active at high wind speeds.

One candidate for enhancing the sea-air enthalpy flux at high wind speeds is sea spray. Riehl (1954, p. 287) was perhaps the first to suggest that sea spray supplies a significant amount of heat for generating and maintaining tropical storms. Laboratory studies (e.g., Mestayer & Lefauconnier 1988), numerical spray droplet models (e.g., Rouault et al. 1991, Edson et al. 1996, Van Eijk et al. 2001), and open-ocean observations (Korolev et al. 1990) all show that sea spray can redistribute enthalpy between the temperature and humidity fields in the marine boundary layer (MBL).

Emanuel (1995b) argued that sea spray could not affect enthalpy transfer because droplets that completely evaporate absorb as much sensible heat as they

give off in latent heat. Several parameterizations of sea spray (e.g., Fairall et al. 1994) have also shown little net enthalpy transfer, and numerical simulations of hurricanes based on these (e.g., Kepert et al. 1999, Uang 1999, Wang et al. 1999) showed little effect of spray on storm intensity. Then Andreas & Emanuel (1999) considered the effect of re-entrant sea spray. After a spray droplet is formed, only about 1% of its mass need evaporate to drop its temperature to the lowest possible value, the wet bulb temperature. If this droplet subsequently falls back into the sea, it cools the ocean and therefore must have effected a net enthalpy transfer to the atmosphere. The authors concluded that a large sea-air enthalpy transfer could result from re-entrant spray. Andreas & Emanuel (2001), for the first time, considered spray effects on momentum transfer and concluded that this effect could be large as well. They developed a new parameterization of air-sea fluxes at high wind speeds and showed that numerical simulations of hurricanes are very sensitive to the details of such parameterizations. Several other numerical simulations (Bao et al. 2000, Wang et al. 2000) confirm that re-entrant sea spray can strongly affect hurricane intensity.

The conclusion of Andreas & Emanuel (2001) that the intensity of simulated hurricanes is very sensitive to the details of the spray formulations as well as to wave-induced drag is disturbing. One inference that follows from this conclusion is that accurate hurricane intensity forecasting will not be possible without coupling the hurricane model to a detailed prognostic surface wave model. Although this may prove to be the case, it is at odds with the findings of Emanuel (1999), who showed that many hurricanes can be accurately hindcasted using a simple coupled model with equal exchange coefficients for enthalpy and momentum. This led to the proposal that during extreme winds, the sea surface becomes self-similar, and all nondimensional transfer coefficients (based on gradient wind speeds) must then be universal constants (Emanuel 2002).

Clearly, this is an important issue that should be resolved by suitably designed field and perhaps laboratory experiments.

5. EFFECTS OF UPPER OCEAN MIXING

Beginning with the observations published by Leipper (1967), it became obvious that hurricanes have a profound effect on the uppermost 200–300 m of the ocean, deepening the mixed layer by many tens of meters, cooling the surface temperature by as much as 5°C, and causing near-inertial surface currents of 1–2 ms^{-1}, detectable at depths up to at least 500 m (Withee & Johnson 1976). Price (1981) established that most of the cooling is owing to entrainment caused by turbulence generated from the strong shear of the near-inertial currents across the base of the mixed layer. This nicely explains the observation that much of the cooling is offset to the right of the storm's track (in the Northern Hemisphere), where the turning of the wind stress as the storm passes resonates with inertial oscillations.

The sensitivity of Equation 8 to local perturbations of sea surface temperature can be seen by noting that under average tropical conditions, a local decrease of

sea surface temperature of only 2.5°C suffices to bring $k_s^* - k$ to zero. (But note that large-scale gradients of sea surface temperature are associated with similar gradients in k, so that $k_s^* - k$ may remain approximately constant over large areas of undisturbed ocean, even though the sea surface temperature varies.) This would suggest that the observed ocean cooling of order 1°C under the storm core could have a significant feedback on hurricane intensity. Sutyrin & Khain (1984), Gallacher et al. (1989), Khain & Ginis (1991), Bender et al. (1993), and Schade & Emanuel (1999) used advanced coupled models to demonstrate that ocean feedback indeed has a first-order effect on hurricane intensity. Emanuel (1999) demonstrated that the intensity of many hurricanes can be accurately predicted using even a very simple atmospheric model coupled to an essentially one-dimensional ocean model (Schade 1997) as long as storms remain unmolested by adverse atmospheric influences, such as environmental wind shear, which has been shown to be a statistically significant predictor of intensity change (DeMaria & Kaplan 1999). An example comparing coupled and uncoupled simulations of a Gulf of Mexico hurricane is shown in Figure 6.

Although it seems clear that accurate prediction of tropical cyclone intensity change requires real-time knowledge of upper ocean thermal structure, in practice, measurements of the upper ocean are few and far between. There is some hope that satellite-based measurements of sea surface altitude, which have been made for about a decade, can be used to make deductions about upper ocean thermal structure (Shay et al. 2000).

6. MOTION

Early observations of cloud motions established that tropical cyclones are highly concentrated vortices that basically move with the background wind in which they are embedded. By the end of the 1940s, however, Davies (1948) and Rossby (1949) had established that vortices alter the vorticity distribution in their environment in such a way as to induce a poleward and westward drift of cyclonic vortices. Broadly, the circulation around tropical cyclones advects air equatorward on their western flanks and poleward on their eastern flanks. Conservation of vorticity implies that equatorward flowing air must acquire cyclonic earth-relative vorticity, whereas poleward flowing air acquires anticyclonic vorticity. The flow associated with these vorticity perturbations acts to advect the tropical cyclone poleward and westward. The early studies assumed that both the vortex flow itself and the flow in which the storms are embedded do not vary with height; such a flow is usually referred to as barotropic flow. Work on the barotropic theory of hurricane motion was advanced by Holland (1983), Chan (1984), DeMaria (1985), Chan & Williams (1987), and Fiorino & Elsberry (1989), among others, and Smith & Ulrich (1990), Smith (1991), and Smith & Weber (1993) developed analytic expressions for the motion of barotropic vortices.

Hurricanes are baroclinic vortices, however, and often occur within large-scale environments that have vertical and lateral wind shear. This shear can have
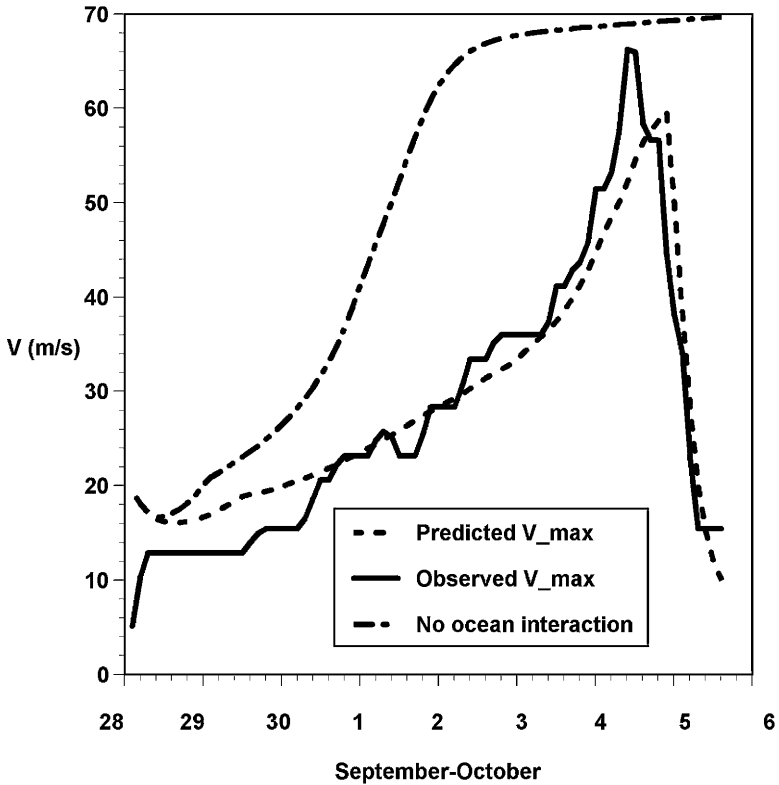
Figure 6   Evolution with time of the observed maximum wind speeds (*solid curve*) in Hurricane Opal of 1995 compared to simulations using a simple model. Simulations using a fixed sea surface temperature (*dash-dot curve*) and coupled with an interactive ocean (*dashed curve*) are shown. From Emanuel (1999).

multiple effects on storm motion. Shapiro (1992) emphasized the connection between shear and the background vorticity distribution, which can have a profound effect on the distribution and intensity of the so-called beta gyres that arise in pure form in barotropic simulations with uniform background vorticity gradients. Wu & Emanuel (1993) emphasized the effect of plumes of low vorticity swept downshear from the vortex at upper levels and later tried to find evidence of these and beta gyres in real data (Wu & Emanuel 1995a,b). The combined effect of a background vorticity gradient and the interaction between the upper-level anticyclone and the lower-level cyclone was also explored by Flatau et al. (1994). Shear can also tilt the cyclonic potential vorticity anomaly associated with hurricanes, giving rise to complex motion (Jones 2000, Smith et al. 2000). All these effects are arguably contained in advanced numerical forecast models, such as the Princeton/GFDL (Geophysical Fluid Dynamics Laboratory) hurricane prediction model (Kurihara

et al. 1998), which in their performance have outrun advances of physical understanding. Today, real-time hurricane track forecasting is based largely on the output of a fairly large number of different numerical models of the atmosphere.

7. GENESIS

No facet of the study of tropical cyclones has proven more vexing than understanding and predicting their genesis. There is not even widespread consensus on the definition of the term, though, very broadly, it is usually applied to systems undergoing a transition from a disturbance not driven by surface fluxes, such as the order 1000-km wave disturbances often observed in the tropics, to a more symmetric, warm-core cyclone with a low pressure center at the surface. From the earliest studies (Riehl 1948), it was recognized that all tropical cyclones originate in some independent disturbance. Bergeron (1954) pointed out that groups of convective showers usually produce cool, anticyclonic outflow at the surface, thus preventing any spontaneous cyclone genesis near the surface. When numerical models are initialized using environments in which the moist convection is statistically equilibrated, a finite amplitude disturbance is required to initiate intensification by wind-surface flux feedback; disturbances that are too weak decay (Rotunno & Emanuel 1987, Emanuel 1989, Dengler & Reeder 1997). This is consistent with the observation that genesis must be triggered by an external disturbance.

Clearly, a necessary condition for genesis is that the potential intensity given by Equation 8 must be sufficiently large. Calculations of this potential maximum wind speed show that it is strongly correlated with ocean surface temperature. Palmén (1948) established that tropical cyclones form only over ocean water with temperatures greater than about 26°C, which supports this conclusion. Gray (1968) showed that genesis only occurs in environments characterized by small vertical shear of the horizontal wind and also favors regions of relatively large cyclonic low-level vorticity. He later established a set of conditions that are apparently necessary (though by no means sufficient) for genesis (Gray 1979). In addition to the two aforementioned factors, Gray argued that larger values of the Coriolis parameter, the heat content of the upper ocean (reflecting the depth of the ocean mixed layer), and the relative humidity of the middle troposphere all favor genesis.

The early investigators, such as Riehl and Bergeron, argued about whether tropical cyclones arise from pre-existing disturbances near the surface, such as fronts, or from disturbances in the upper troposphere. Later observations showed that there are many routes to genesis, including nearly classic baroclinic development (Bosart & Bartlo 1991), interaction of easterly waves or other low-level disturbances with tropical upper tropospheric disturbances (Ramage 1959, Sadler 1976, Montgomery & Farrell 1993), and, possibly, accumulation of wave energy in diffluent large-scale flow (Shapiro 1977, Sobel & Bretherton 1999).

Another body of theory developed around the idea that patches of high vorticity associated with individual convective systems can, under certain circumstances,

merge to form a more powerful incipient cyclone. This idea may have started with Fujiwhara's 1923[4] proposal that genesis involves the fusion of several small vortices and has been recently revived (Ritchie & Holland 1993, Simpson et al. 1997). Montgomery & Enagonio (1998) and Moller & Montgomery (1999, 2000) showed that small-scale patches of vorticity introduced into the flow field of a larger-scale vortex are quickly axisymmetrized, feeding their energy into the vortex scale flow in the process. This suggests that mesoscale convective systems that develop outside the eyewall may help intensify the storm as a whole.

The central problem in genesis is the transformation of an existing disturbance into a system operating on the feedback between surface enthalpy fluxes and surface wind. Any complete theory must account for the fact that such transformations are relatively unusual and, in any event, only occur under the conditions reviewed by Gray (1979). Bergeron (1954) had concluded that, under normal circumstances, convective downdrafts quench any nascent tendency for the boundary layer entropy to increase; he suggested that if, by some means, the surface cyclone could be made strong enough, the inward Ekman drift would overcome the anticyclonic outflow, leading to a positive feedback between surface enthalpy flux and wind, and transformation into a warm-core system. But it has become clear from a series of numerical experiments (Emanuel 1989, Emanuel 1995a) and a field experiment (Emanuel 1994, Bister & Emanuel 1997) that a necessary condition for genesis is the establishment of an order 100-km-wide column of nearly saturated air in the core of the system, so that cumulus convection rising into this air cannot produce low entropy downdrafts driven by evaporating rain. Any environmental influence that disrupts the formation of such a saturated column will prevent genesis and weaken any existing system. Clearly, the ventilation of low entropy air in the middle troposphere through a nascent system will have this effect, as first pointed out by Simpson & Riehl (1958); this nicely explains why vertical shear is inimical to genesis. In axisymmetric models, the establishment of an order 100-km-wide saturated column appears also to be a sufficient condition for genesis (Emanuel 1995a). An important remaining question is how such a column is established; the various mechanisms described in the previous paragraph could all work in this direction. The same axisymmetric models show that a cyclonic circulation of sufficient strength at the surface can ultimately give rise to genesis after a gestation period in which the friction and downdrafts weaken the circulation, while at the same time frictionally driven inflow and associated ascent moistens a deep column in the core of the system. But detailed observations of evolving clusters of clouds (Davidson 1995a,b) and of Hurricane Guillermo in the eastern North Pacific in 1991 (Bister & Emanuel 1997) suggest that in these developments, the saturation was achieved by evaporation of rain falling from stratiform outflow clouds associated with the cumulus convection, and that downward advection of angular momentum in the evaporatively driven downdraft was an important ingredient in the subsequent genesis. It is by no means clear, however, that such a mechanism is at work in all or

---

[4]Cited in Bergeron (1954, page 144) but no detailed reference is given.

even most cases of genesis. This conclusion reflects the paucity of field experiments dedicated to the problem of tropical cyclone genesis. Clearly, we have a long way to go in understanding genesis.

8. SUBSTRUCTURE OF TROPICAL CYCLONES

The earliest radar images of tropical cyclones (Wexler 1947) showed the beautiful spiral rainbands than accompany them. Since then, there has been a vigorous effort to characterize and understand mesoscale (order 100 km) structure in such storms. Radar, satellite, and aircraft observations have revealed a plethora of mesoscale structures in tropical cyclones. We review progress in understanding these in the following subsections.

8.1 Spiral Rainbands

Spiral rainbands were probably first noticed on radar, and many theories have been formulated to explain them. They consist of bands of cumulus clouds, some tens of kilometers wide and often precipitating, that spiral in toward the center of the storms, sometimes connecting with the eyewall. Senn & Hiser (1959) noticed in radar observations that spiral bands seem to form near the eyewall and propagate outward, assuming a quasi-stationary position with respect to the storm. They also noted that the spirals were not organizations of pre-existing convective cells; instead, cells tend to develop and decay within the bands. The first theory to explain these observations was advanced by Abdullah (1966). He proposed that spiral bands represent outward propagating inertia-gravity waves, originating in the storm core. His hypothesis was bolstered by analysis of spiral bands that appeared in early three-dimensional numerical simulations (Dierecks & Anthes 1976), which showed that they were indeed inertia-gravity waves, and by a linear stability analysis of baroclinic circular vortices by Kurihara (1976). The inertia-gravity waves in the Dierecks & Anthes study may have been exaggerated by the imposition of a rigid upper boundary in the simulation, which does not permit the upward propagation of wave energy that would otherwise occur to some degree. Willoughby (1977; 1978a,b; 1979) showed that inward propagating inertia-gravity waves would be amplified by conservation of wave activity, eventually being absorbed in the eyewall and at a critical level in the outflow. He also argued that waves could be excited at the periphery of storms by their interaction with environments in which the wind varies with altitude or in the horizontal. In a later paper, Willoughby et al. (1984b) suggested that the principal spiral rainband that is observed to remain quasi-stationary with respect to the storm might be formed at the boundary between recirculating air in the core and air that flows through the system in outer regions.

Another hypothesis for spiral rainbands arose as a result of laboratory experiments performed by Faller (1963), which showed that laminar Ekman boundary layer flow spontaneously develops spiral bands. These bands were explained by Lilly (1966) as manifestations of two different types of linear instability; one is

a Rayleigh-type instability resulting from an unstable distribution of horizontal vorticity in the boundary layer, whereas the other is more nearly akin to inertial instability. Fung (1977) proposed that spiral rainbands arise from a cooperative interaction between such boundary layer instabilities and deep moist convection.

Yet another theory of spiral bands was proposed by McDonald (1968), who suggested that they were manifestations of Rossby waves that propagate on the strong radial vorticity gradient outside the core. Montgomery (1997) developed a complete theory of vortex Rossby waves, and Guinn & Schubert (1993) also suggested that the spiral bands are a result of breaking Rossby waves, leading to the production of long, thin filaments of vorticity that spin out from the eyewall to form the spiral bands.

Much of the extant theory of spiral bands has been worked out for adiabatic motions, reflecting our poor understanding of the interaction between cumulus convection and larger-scale circulations. The relevance of such theories to the observed phenomenon has been questioned by Schade (1994), who pointed out that vertical motions driven by condensation and evaporation produce such strong sources and sinks of vorticity as to render suspect theories based on its conservation; indeed, the first-order balance is between diabatic production and frictional dissipation of potential vorticity.

Improved observations from reconnaissance aircraft led to better analyses of the structure and behavior of spiral bands. By the early 1980s, the mesoscale structure of the bands had been well documented (Barnes et al. 1983). Detailed distributions of moist entropy and airflow around spiral bands were published by Powell (1990a,b); these showed that, like squall lines, there are strong interactions between rain-cooled air flowing out of the convection at low levels and strong boundary layer wind shear. Robe & Emanuel (2001) proposed that spiral rainbands are essentially squall lines whose local orientation is dictated by the direction of the boundary layer wind shear, such that the component of shear normal to the bands is optimum in the sense defined by Rotunno et al. (1988).

8.2 Concentric Eyewalls

Radar imagery and aircraft data also reveal the existence of nearly circular rainbands that tend to form outside the eyewall and then contract inward, eventually replacing the existing eyewall. Double eyewalls had been noticed on radar images at least as early as 1961 (Jordan & Schatzle 1961), but the first thorough analyses were presented by Willoughby et al. (1982), who also showed that the outer eyewalls are associated with secondary wind maxima, which amplify as the outer eyewalls contract, eventually becoming the dominant wind maximum. This eyewall replacement cycle can be responsible for large fluctuations in storm intensity and seems to be a feature of particularly intense storms. It is thought, for example, that the exceptional destructiveness of Hurricane Andrew in south Florida in 1992 was partially owing to the timing of its landfall with respect to an eyewall cycle (Willoughby & Black 1996). Hawkins (1983) suggested that outer eyewalls might form as a consequence of the interaction of the low-level storm circulation

with mountainous islands. Numerical models have successfully simulated eyewall cycles (Lord et al. 1984, Willoughby et al. 1984a), which seem to be more intense when ice physics are included in the model. In models, the evolution of concentric eyewalls appears to depend on the same feedback between wind and surface enthalpy flux that drives the storm as a whole (Emanuel 1995a).

8.3 Secondary Vortices

Detailed reconstructions of tropical cyclone wind fields, made possible with ground-based and airborne Doppler radar, as well as aircraft data and examination of storm damage, show that tropical cyclones are frequently accompanied by small-scale, transient vortices usually embedded in the eyewall. Some of these may significantly increase the damage done by strong winds (Willoughby & Black 1996). Lewis & Hawkins (1982) described eyewalls that seemed to consist of a series of line segments forming squares or polygons, and by the mid 1980s, Marks & Houze (1984) had documented the existence of mesocyclones in the eyewall, using airborne Doppler radar observations. Small-scale velocity structures are often made visible as tilted striations on the inner edge of the eyewall cloud (Bluestein & Marks 1987). The first theoretical studies of these phenomena were published only very recently (Schubert et al. 1999, Kossin et al. 2000) and strongly suggest that at least some of these vortices result from the unstable distribution of vorticity that results from the contraction of the eyewall.

Forecasters knew from early experience that landfalling tropical cyclones are often accompanied by outbreaks of tornadoes, especially in certain quadrants of the storm (Hill et al. 1966). Later research (McCaul 1991) suggests that strong wind shear in the boundary layer, associated with strongly curved hodographs, is responsible for producing convective storms that resemble the tornado-producing superstorms found in the American plain states, in spite of the absence of the large reservoirs of potential energy that accompany most tornadic storms.

9. TROPICAL CYCLONES AND CLIMATE

Bergeron (1954) was probably the first to speculate about the dependence of tropical cyclone activity on climate. Namias (1955) showed that there were strong correlations between interannual fluctuations of Atlantic hurricane activity and changes in the general circulation, particularly in the pattern of long waves in the west-to-east flow of air prevalent in middle latitudes. Shapiro (1982a,b) demonstrated a clear connection between interannual fluctuations in Atlantic hurricane activity and other climate signals, including a measure of the phase of the quasi-biennial oscillation and sea surface temperatures west of Africa. Gray (1984) showed a strong connection between Atlantic hurricane activity and El Niño, and by the early 1990s a strong correlation was found between hurricane activity and rainfall in sub-Saharan Africa (Landsea & Gray 1992). Saunders & Harris (1997) showed that the particularly active 1995 Atlantic hurricane season was related

to exceptionally warm sea surface temperatures, though Shapiro & Goldenberg (1998) noted that most of this signal might result from a connection between sea surface temperature gradients and vertical wind shear, with only a relatively small part owing to the direct influence of sea surface temperature on cyclone formation. Goldenberg & Shapiro (1996) also argued that the physical link between Atlantic hurricane activity and phenomena such as El Niño and sub-Saharan rainfall is through the effect of these phenomena on vertical wind shear over the genesis regions of the North Atlantic. By the 1980s, the Colorado State University group had started using these signals in an attempt to provide seasonal forecasts of Atlantic tropical cyclone activity (Gray et al. 1992). In the last decade of the century, a strong relationship between Atlantic hurricane activity and the North Atlantic Oscillation was discovered (Goldenberg et al. 2001), giving some hope that decadal variations in hurricane activity might be partially anticipated.

Although there has been a flurry of research on the relationship between Atlantic tropical cyclone activity and climate, there is a comparative paucity of similar work on tropical cyclones in other parts of the world. Clearly, this issue is ripe for research.

By the end of the 1980s, it was becoming apparent that average global surface temperature was increasing, perhaps in response to anthropogenically induced increases in greenhouse gases, and the effect of global warming on hurricane activity became a concern. Emanuel (1987) argued that increasing greenhouse gases alter the energy balance at the surface of tropical oceans in such a way as to require a greater turbulent enthalpy flux out of the ocean, thereby requiring a greater degree of thermodynamic disequilibrium between the tropical oceans and atmosphere. Using a single-column radiative-convective model, he argued that the potential intensity of tropical cyclones evaluated using Equation 8 would increase by approximately 3.5 ms^{-1} for each 1°C increase in tropical sea surface temperatures, and he supported this claim with a calculation of potential intensity from a global climate model subjected to a doubling of atmospheric CO_2. Subsequent work by Knutson et al. (1998), using a high-resolution tropical cyclone model with boundary conditions from a global climate model, gave a similar estimate for the increase in tropical cyclone intensity that might arise as a consequence of global warming. But the problem of how global climate change might affect the frequency of tropical cyclones remains largely unsolved. Global climate models (GCMs) appear to give disparate results. For example, a study by Haarsma et al. (1992), using the GCM run by the British Meteorological Office, shows an increase in both the intensity and frequency of tropical cyclones, but an analysis by Broccoli & Manabe (1990), using the Princeton/GFDL model, shows ambiguous results, with an increase in tropical cyclone activity if cloud-radiation feedback is not included and a decrease in activity otherwise. But it is clear from all these studies that even were the worst scenarios of global warming realized, the expected changes in tropical cyclone activity would be small compared to those arising from the kind of natural variability described earlier in this section, at least for the next 50 years. On longer timescales, the effects of global warming might be more serious.

Perhaps the most promising route to understanding the relationship between long-term climate change and changes in tropical cyclone activity is through examination of the geological record, as Bergeron (1954) first suggested. The budding new field of paleotempestology is just beginning to show how tropical cyclone activity varies on timescales of centuries to millennia. For example, Liu & Fearn (1993) have taken a series of sediment cores from near-shore lakes and swamps along the U.S. Gulf coast and have been able to deduce the timings of strong landfalling storms by observing sand layers in the cores and carbon-dating them from the surrounding organic matter. They have, in the past decade, developed a record of strong landfalling storms going back more than 3000 years at some sites. Work like this, if extended in space and further back into the past, may reveal how tropical cyclone activity changes on very long timescales, offering an opportunity to understand how such activity is related to global and regional climate change on a variety of timescales.

Although tropical cyclones are usually considered to respond passively to climate changes on many timescales, it may be that they are active players in phenomena like El Niño and the North Atlantic Oscillation. The author (Emanuel 2001) has argued that much of the thermohaline circulation is actually driven by global tropical cyclone activity. If this proves to be the case, then the variation of tropical cyclone activity with climate may be integral to the physics of a wide variety of climate phenomena. A simple climate model constructed by the author (Emanuel 2002) indeed suggests that accounting for the control of the oceanic poleward heat flux by tropical cyclones might explain such mysteries as high-latitude warmth during the Cretaceous and early Eocene and sudden climate transitions evident in ice cores and deep sea sediment records. Thus, far from being isolated freaks of nature, tropical cyclones may be integral to the earth's climate system.

The *Annual Review of Earth and Planetary Science* is online at
http://earth.annualreviews.org

LITERATURE CITED

Abdullah AJ. 1966. The spiral bands of a hurricane: a possible dynamic explanation. *J. Atmos. Sci.* 23:367–75

Andreas EL, Emanuel KA. 1999. *Effects of sea spray on tropical cyclone intensity*. Presented at 23rd Conf. Hurric. Trop. Meteorol., Dallas, TX

Andreas EL, Emanuel KA. 2001. Effects of sea spray on tropical cyclone intensity. *J. Atmos. Sci.* 58:3741–51

Bao J-W, Wilczak JM, Choi JK, Kantha LH. 2000. Numerical simulations of air-sea interaction under high wind conditions using a coupled model: a study of hurricane development. *Mon. Weather Rev.* 128:2190–210

Barnes GM, Zipser EJ, Jorgensen DP, Marks FD Jr. 1983. Mesoscale and convective structure of a hurricane rainband. *J. Atmos. Sci.* 40:2125–37

Bender MA, Ginis IY, Kurihara Y. 1993. Numerical simulations of tropical cyclone-ocean interaction with a high resolution coupled model. *J. Geophys. Res.* 98:23245–63

Bergeron T. 1954. The problem of tropical hurricanes. *Q. J. R. Meteorol. Soc.* 80:131–64

Bister M, Emanuel KA. 1997. The genesis of Hurricane Guillermo: TEXMEX analyses and a modeling study. *Mon. Weather Rev.* 125:2662–82

Bister M, Emanuel KA. 1998. Dissipative heating and hurricane intensity. *Meteorol. Atmos. Phys.* 50:233–40

Bluestein HB, Marks FD Jr. 1987. On the structure of the eyewall of Hurricane "Diana" (1984): comparison of radar and visual characteristics. *Mon. Weather Rev.* 115:2542–52

Bosart LF, Bartlo JA. 1991. Tropical storm formation in a baroclinic environment. *Mon. Weather Rev.* 119:1979–2013

Broccoli AJ, Manabe S. 1990. Can existing climate models be used to study anthropogenic changes in tropical cyclone climate? *Geophys. Res. Lett.* 17:1917–20

Chan C-L. 1984. Observational study of the physical processes responsible for tropical cyclone motion. *J. Atmos. Sci.* 41:1036–48

Chan C-L, Williams RT. 1987. Analytical and numerical studies of the beta-effect in tropical cyclone motion, Pt. 1. Zero mean flow. *J. Atmos. Sci.* 44:1257–65

Davidson NE. 1995a. Vorticity budget for AMEX. Part I: diagnostics. *Mon. Weather Rev.* 123:1620–35

Davidson NE. 1995b. Vorticity budget for AMEX. Part II: simulations of monsoon onset, midtropospheric cyclones and tropical cyclone behavior. *Mon. Weather Rev.* 123:1636–59

Davies TV. 1948. Rotatory flow on the surface of the earth. Part I. Cyclostrophic motion. *Philos. Mag.* 39:482–91

DeMaria M. 1985. Tropical cyclone motion in a nondivergent barotropic model. *Mon. Weather Rev.* 137:1199–210

DeMaria M, Kaplan J. 1999. An updated statistical hurricane intensity prediction scheme (SHIPS) for the Atlantic and eastern North Pacific basins. *Weather Forecast.* 14:326–37

Dengler K, Reeder MJ. 1997. The effects of convection and baroclinicity on the motion of tropical-cyclone-like vortices. *Q. J. R. Meteorol. Soc.* 123:699–725

Dierecks JW, Anthes RA. 1976. Diagnostic studies of spiral rainbands in a nonlinear hurricane model. *J. Atmos. Sci.* 33:959–75

Edson JB, Anquentin S, Mestayer PG, Sini JF. 1996. Spray droplet modeling: 2. An interactive Eulerian-Lagrangian model of evaporating spray droplets. *J. Geophys. Res.* 101:1279–93

Emanuel KA. 1986. An air-sea interaction theory for tropical cyclones. Part I. *J. Atmos. Sci.* 42:1062–71

Emanuel KA. 1987. The dependence of hurricane intensity on climate. *Nature* 326:483–85

Emanuel KA. 1988. The maximum intensity of hurricanes. *J. Atmos. Sci.* 45:1143–55

Emanuel KA. 1989. The finite-amplitude nature of tropical cyclogenesis. *J. Atmos. Sci.* 46:3431–56

Emanuel KA. 1994. The physics of tropical cyclogenesis over the eastern Pacific. In *Tropical Cyclone Disasters*, ed. J Lighthill, Z Zhemin, G Holland, K Emanuel. Beijing: Peking Univ. Press. 588 pp.

Emanuel KA. 1995a. The behavior of a simple hurricane model using a convective scheme based on subcloud-layer entropy equilibrium. *J. Atmos. Sci.* 52:3959–68

Emanuel KA. 1995b. Sensitivity of tropical cyclones to surface exchange coefficients and a revised steady-state model incorporating eye dynamics. *J. Atmos. Sci.* 52:3969–76

Emanuel KA. 1997. Some aspects of hurricane inner-core dynamics and energetics. *J. Atmos. Sci.* 54:1014–26

Emanuel KA. 1998. The power of a hurricane. An example of reckless driving on the information superhighway. *Weather* 54:107–8

Emanuel KA. 1999. Thermodynamic control of hurricane intensity. *Nature* 401:665–69

Emanuel KA. 2000. A statistical analysis of tropical cyclone intensity. *Mon. Weather Rev.* 128:1139–52

Emanuel KA. 2001. The contribution of tropical cyclones to the oceans' meridional heat transport. *J. Geophys. Res.* 106:14771–81

Emanuel K. 2002. A simple model of multiple

climate regimes. *J. Geophys. Res.* 107: doi: 10.1029/2001JD001002

Emanuel K. 2003. A similarity hypothesis for air-sea exchange at extreme wind speeds. *J. Atmos. Sci.* 59:In press

Emanuel KA, Rotunno R. 1989. Polar lows as arctic hurricanes. *Tellus A* 41:1–17

Emanuel KA, Speer K, Rotunno R, Srivastava R, Molina M. 1995. Hypercanes: a possible link in global extinction scenarios. *J. Geophys. Res.* 100:13755–65

Fairall CW, Kepert JD, Holland GJ. 1994. The effect of sea spray on surface energy transports over the ocean. *Global Atmos. Ocean Syst.* 2:121–42

Faller AJ. 1963. An experimental study of the instability of the laminar Ekman boundary layer. *J. Fluid Mech.* 15:560–76

Fiorino M, Elsberry RL. 1989. Contributions to tropical cyclone motion by small, medium, and large scales in the initial vortex. *Mon. Weather Rev.* 117:721–27

Flatau M, Schubert WH, Stevens DE. 1994. The role of baroclinic processes in tropical cyclone motion: the influence of vertical tilt. *J. Atmos. Sci.* 51:2589–601

Frank WM. 1977a. Structure and energetics of the tropical cyclone, pt. 1, storm structure. *Mon. Weather Rev.* 105:1119–35

Frank WM. 1977b. Structure and energetics of the tropical cyclone, pt. 2: dynamics and energetics. *Mon. Weather Rev.* 105:1136–50

Fung IY-S. 1977. *The organization of spiral rainbands in a hurricane*. Sc.D. thesis. MIT, Cambridge, MA. 140 pp.

Gallacher PC, Rotunno R, Emanuel KA. 1989. *Tropical cyclogenesis in a coupled ocean-atmosphere model*. Presented at 18th Conf. Hurric. Trop. Meteorol., Miami, FL

Goldenberg SB, Landsea CW, Mestas-Nuñez AM, Gray WM. 2001. The recent increase in Atlantic hurricane activity: causes and implications. *Science* 293:474–79

Goldenberg SB, Shapiro LJ. 1996. Physical mechanisms for the association of El Niño and West African rainfall with Atlantic major hurricane activity. *J. Climate* 9:1169–87

Gray WM. 1968. Global view of the origin of tropical disturbances and storms. *Mon. Weather Rev.* 96:669–700

Gray WM. 1979. Hurricanes: their formation, structure, and likely role in the tropical circulation. In *Meteorology Over the Tropical Oceans*, ed. DB Shaw, pp. 155–218. Reading, UK: R. Meteorol. Soc.

Gray WM. 1984. Atlantic seasonal hurricane frequency. Part I: El Niño and 30 mb quasi-biennial oscillation influences. *Mon. Weather Rev.* 112:1649–68

Gray WM, Landsea C, Mielke PWJ, Berry KJ. 1992. Predicting Atlantic seasonal hurricane activity 6–11 months in advance. *Weather Forecast.* 7:440–55

Greeneart GL, Larsen SE, Hansen F. 1987. Measurements of the wind stress, heat flux and turbulence intensity during storm conditions over the North Sea. *J. Geophys. Res.* 92:13127–39

Guinn TA, Schubert WH. 1993. Hurricane spiral bands. *J. Atmos. Sci.* 50:3380–403

Haarsma RJ, Mitchell JFB, Senior CA. 1992. Tropical disturbances in a GCM. *Clim. Dyn.* 8:247–57

Hawkins HF. 1983. Hurricane Allen and island obstacles. *J. Atmos. Sci.* 40:1360–62

Hawkins HF, Imbembo SM. 1976. The structure of a small, intense hurricane—Inez 1966. *Mon. Weather Rev.* 44:418–42

Hill EL, Malkin W, Schulz WA. 1966. Tornadoes associated with cyclones of tropical origin—practical features. *J. Appl. Meteor.* 5:745–63

Holland G. 1983. Tropical cyclone motion: environmental interaction plus a beta-effect. *J. Atmos. Sci.* 40:328–42

Jones SC. 2000. The evolution of vortices in vertical shear. Part III: baroclinic vortices. *Q. J. R. Meteorol. Soc.* 126:3161–85

Jordan CL, Schatzle FJ. 1961. The "double eye" of Hurricane Donna. *Mon. Weather Rev.* 89:354–56

Jorgensen DP. 1984. Mesoscale and convective-scale characteristics of mature hurricanes. Part I: general observations by research aircraft. *J. Atmos. Sci.* 41:1268–85

Jorgensen DP, Zipser EJ, LeMone MA. 1985. Vertical motions in intense hurricanes. *J. Atmos. Sci.* 42:839–56

Kepert JD, Fairall CW, Bao J-W. 1999. Modeling the interaction between the atmospheric boundary layer and evaporating sea spray droplets. In *Air-Sea Exchange: Physics, Chemistry and Dynamics*, ed. GL Greenaert, pp. 369–409. Dordrecht, The Netherlands: Kluwer

Khain A, Ginis I. 1991. The mutual response of a moving tropical cyclone and the ocean. *Beitr. Phys. Atmos.* 64:125–41

Kleinschmidt E Jr. 1951. Gundlagen einer theorie des tropischen zyklonen. *Arch. Meteorol. Geophys. Bioklimatol. Ser. A* 4:53–72

Knutson TR, Tuleya RE, Kurihara Y. 1998. Simulated increase of hurricane intensities in a CO_2-warmed climate. *Science* 279:1018–20

Korolev VS, Petrichenko SA, Pudov VD. 1990. Heat and moisture exchange between the ocean and atmosphere in tropical storms Tess and Skip. *Sov. Meteorol. Hydrol.* 3:92–94

Kossin JP, Schubert WH, Montgomery MT. 2000. Unstable interactions between a hurricane's primary eyewall and a secondary ring of enhanced vorticity. *J. Atmos. Sci.* 57:3893–917

Kurihara Y. 1976. On the development of spiral bands in a tropical cyclone. *J. Atmos. Sci.* 33:940–58

Kurihara Y, Tuleya RE, Bender MA. 1998. The GFDL hurricane prediction system and its performance in the 1995 hurricane season. *Mon. Weather Rev.* 126:1306–22

Landsea CW, Gray WM. 1992. The strong association between western Sahelian monsoon rainfall and intense Atlantic hurricanes. *J. Climate* 5:435–53

Leipper DF. 1967. Observed ocean conditions and Hurricane Hilda, 1964. *J. Atmos. Sci.* 24:182–96

Lewis BM, Hawkins HF. 1982. Polygonal eye walls and rainbands in hurricanes. *Bull. Am. Meteorol. Soc.* 63:1294–301

Lilly DK. 1966. On the instability of Ekman boundary flow. *J. Atmos. Sci.* 23:481–94

Liu K-B, Fearn ML. 1993. Lake-sediment record of late Holocene hurricane activities from coastal Alabama. *Geology* 21:793–96

Lord SJ, Willoughby HE, Piotrowicz JM. 1984. Role of a parameterized ice phase microphysics in an axisymmetric, nonhydrostatic tropical cyclone model. *J. Atmos. Sci.* 41:2836–48

Marks FD Jr, Houze RA. 1984. Airborne Doppler radar observations in Hurricane Debby. *Bull. Am. Meteorol. Soc.* 65:569–82

Marks FD Jr, Houze RA. 1987. Inner core structure of Hurricane Alicia from airborne Doppler radar observations. *J. Atmos. Sci.* 44:1296–317

McCaul EW Jr. 1991. Buoyancy and shear characteristics of hurricane-tornado environments. *Mon. Weather Rev.* 119:1954–78

McDonald NJ. 1968. The evidence for the existence of Rossby-like waves in the hurricane vortex. *Tellus* 20:138–50

Mestayer PG, Lefauconnier C. 1988. Spray droplet generation, transport, and evaporation in a wind wave tunnel during the Humidity Exchange over the Sea Experiments in the Simulation Tunnel. *J. Geophys. Res.* 93:572–86

Molinari J, Moore PK, Idone VP, Henderson RW, Saljoughy AB. 1994. Cloud-to-ground lightning in Hurricane Andrew. *J. Geophys. Res.* 99:16665–76

Moller JD, Montgomery MT. 1999. Vortex Rossby waves and hurricane intensification in a barotropic model. *J. Atmos. Sci.* 56:1674–87

Moller JD, Montgomery MT. 2000. Tropical cyclone evolution via potential vorticity anomalies in a three-dimensional balance model. *J. Atmos. Sci.* 57:3366–87

Montgomery MT. 1997. A theory for vortex Rossby-waves and its application to spiral bands and intensity changes in hurricanes. *Q. J. R. Meteorol. Soc.* 123:435–65

Montgomery MT, Enagonio J. 1998. Tropical cyclogenesis via convectively forced vortex

Rossby waves in a three-dimensional quasi-geostrophic model. *J. Atmos. Sci.* 55:3176–207

Montgomery MT, Farrell BF. 1993. Tropical cyclone formation. *J. Atmos. Sci.* 50:285–310

Namias J. 1955. Tropical cyclones related to the atmosphere's general circulation. *Trans. NY Acad. Sci. Ser. II* 17:346–49

Neumann C. 1993. Global overview. In *Global Guide to Tropical Cyclone Forecasting WMO/TD-560*, ed. GJ Holland, pp. 3.1–3.46. Geneva: World Meteorol. Org.

Ooyama K. 1969. Numerical simulation of the life-cycle of tropical cyclones. *J. Atmos. Sci.* 26:3–40

Palmén E. 1948. On the formation and structure of tropical hurricanes. *Geophysica* 3:26–39

Pielke RA. 1990. *The Hurricane*. New York: Routledge. 228 pp.

Powell MD. 1990a. Boundary layer structure and dynamics in outer hurricane rainbands. Part I: mesoscale rainfall and kinematic structure. *Mon. Weather Rev.* 118:891–917

Powell MD. 1990b. Boundary layer structure and dynamics in outer hurricane rainbands. Part II: downdraft modification and mixed layer recovery. *Mon. Weather Rev.* 118:918–38

Price JF. 1981. Upper ocean response to a hurricane. *J. Phys. Ocean.* 11:153–75

Ramage CS. 1959. Hurricane development. *J. Meteorol.* 16:227–37

Reale O, Atlas R. 2001. Tropical cyclone-like vortices in the extratropics: observational evidence and synoptic analysis. *Weather Forecast.* 16:7–34

Riehl H. 1948. On the formation of typhoons. *J. Meteorol.* 5:247–64

Riehl H. 1950. A model for hurricane formation. *J. Appl. Phys.* 21:917–25

Riehl H. 1954. *Tropical Meteorology*. New York: McGraw-Hill. 392 pp.

Ritchie EA, Holland GJ. 1993. On the interaction of tropical-cyclone scale vortices. II: interacting vortex patches. *Q. J. R. Meteorol. Soc.* 119:1363–97

Robe FR, Emanuel K. 2001. The effect of vertical wind shear on radiative-convective equilibrium states. *J. Atmos. Sci.* 58:1427–45

Rosenthal SL. 1971. The response of a tropical cyclone model to variations in boundary layer parameters, initial conditions, lateral boundary conditions and domain size. *Mon. Weather Rev.* 99:767–77

Rossby C-G. 1949. On a mechanism for the release of potential energy in the atmosphere. *J. Meteorol.* 6:164–80

Rotunno R, Emanuel KA. 1987. An air-sea interaction theory for tropical cyclones. Part II. *J. Atmos. Sci.* 44:542–61

Rotunno R, Klemp JB, Weisman ML. 1988. A theory for strong, long-lived squall lines. *J. Atmos. Sci.* 45:463–85

Rouault MP, Mestayer PG, Schiestel R. 1991. A model of evaporating spray droplet dispersion. *J. Geophys. Res.* 96:7181–200

Sadler JC. 1976. A role of the tropical upper tropospheric trough in early season typhoon development. *Mon. Weather Rev.* 104:1266–78

Saunders MA, Harris AR. 1997. Statistical evidence links exceptional 1995 Atlantic hurricane season to record sea warming. *Geophys. Res. Lett.* 24:1255–58

Schade LR. 1994. Comments on "hurricane spiral bands." *J. Atmos. Sci.* 51:3543–44

Schade LR. 1997. *A physical interpretation of SST-feedback.* Presented at 22nd Conf. Hurric. Trop. Meteorol., Boston, MA

Schade LR, Emanuel KA. 1999. The ocean's effect on the intensity of tropical cyclones: results from a simple coupled atmosphere-ocean model. *J. Atmos. Sci.* 56:642–51

Schubert WH, Montgomery MT, Taft RK, Guinn TA, Fulton SR, et al. 1999. Polygonal eyewalls, asymmetric eye contraction, and potential vorticity mixing in hurricanes. *J. Atmos. Sci.* 56:1197–223

Senn HV, Hiser HW Jr. 1959. On the origin of hurricane spiral rainbands. *J. Meteorol.* 16:419–26

Shapiro LJ. 1977. Tropical storm formation from easterly waves: a criterion for development. *J. Atmos. Sci.* 34:1007–21

Shapiro LJ. 1982a. Hurricane climatic fluctuations. Part I: patterns and cycles. *Mon. Weather Rev.* 110:1007–13

Shapiro LJ. 1982b. Hurricane climatic fluctuations. Part II: relation to large-scale circulation. *Mon. Weather Rev.* 110:1014–23

Shapiro LJ. 1992. Hurricane vortex motion and evolution in a three-layer model. *J. Atmos. Sci.* 49:140–53

Shapiro LJ, Goldenberg SB. 1998. Atlantic sea surface temperatures and tropical cyclone formation. *J. Climate* 6:677–99

Shay LK, Goni GJ, Black PG. 2000. Effects of a warm oceanic feature on Hurricane Opal. *Mon. Weather Rev.* 128:1366–83

Simpson J, Ritchie EA, Holland G, Halverson J, Stewart S. 1997. Mesoscale interactions in tropical cyclone genesis. *Mon. Weather Rev.* 125:2643–61

Simpson RH, Riehl H. 1958. *Mid-tropospheric ventilation as a constraint on hurricane development and maintenance*. Presented at Tech. Conf. Hurric., Miami, FL

Smith RK. 1991. An analytic theory of tropical-cyclone motion in a barotropic shear flow. *Q. J. R. Meteorol. Soc.* 117:685–714

Smith RK, Ulrich W. 1990. An analytical theory of tropical cyclone motion using a barotropic model. *J. Atmos. Sci.* 47:1973–86

Smith RK, Ulrich W, Sneddon G. 2000. On the dynamics of hurricane-like vortices in vertical-shear flows. *Q. J. R. Meteorol. Soc.* 126:2653–70

Smith RK, Weber H. 1993. An extended analytic theory of tropical-cyclone motion in a barotropic shear flow. *Q. J. R. Meteorol. Soc.* 119:1149–66

Sobel AH, Bretherton CS. 1999. Development of synoptic-scale disturbances over the summertime tropical northwest Pacific. *J. Atmos. Sci.* 56:3106–27

Sutyrin GG, Khain AP. 1984. Effect of the ocean-atmosphere interaction on the intensity of a moving tropical cyclone. *Izvest. Atmos. Ocean. Phys.* 20:697–703

Twitchell PF, Rasmussen EA, Davidson KL, eds. 1989. *Polar and Arctic Lows*. Hampton, VA: Deepak. 421 pp.

Uang C-L. 1999. *Impacts of sea spray and oceanic response on the development of tropical cyclones*. Presented at 23rd Conf. Hurric. Trop. Meteorol., Dallas, TX

Van Eijk AMJ, Tranchant BS, Mestayer PG. 2001. SeaCluse: numerical simulation of evaporating sea spray droplets. *J. Geophys. Res.* 106:2573–88

Wang Y, Kepert JD, Holland G. 1999. *The impact of sea spray evaporation on tropical cyclone intensification*. Presented at 23rd Conf. Hurric. Trop. Meteorol., Dallas, TX

Wang Y, Kepert JD, Holland G. 2000. *On the effect of sea spray evaporation on tropical cyclone boundary-layer structure and intensity*. Presented at 23rd Conf. Hurric. Trop. Meteorol., Dallas, TX

Weatherford CL, Gray WM. 1988. Typhoon structure as revealed by aircraft reconnaissance. Part I: data analysis and climatology. *Mon. Weathar Rev.* 116:1032–43

Wexler H. 1947. Structure of hurricanes as determined by radar. *Ann. NY Acad. Sci.* 48:821–44

Willoughby HE. 1977. Inertia-buoyancy waves in hurricanes. *J. Atmos. Sci.* 34:1028–39

Willoughby HE. 1978a. Possible mechanism for the formation of hurricane rainbands. *J. Atmos. Sci.* 35:838–48

Willoughby HE. 1978b. Vertical structure of hurricane rainbands and their interaction with the mean vortex. *J. Atmos. Sci.* 35:849–58

Willoughby HE. 1979. Excitation of spiral bands in hurricanes by interaction between the symmetric mean vortex and a shearing environmental steering current. *J. Atmos. Sci.* 36:1226–35

Willoughby HE, Black PG. 1996. Hurricane Andrew in Florida: dynamics of a disaster. *Bull. Am. Meteorol. Soc.* 77:543–49

Willoughby HE, Clos JA, Shoreibah MG. 1982. Concentric eyes, secondary wind maxima, and the evolution of the hurricane vortex. *J. Atmos. Sci.* 39:395–411

Willoughby HE, Jin H-L, Lord SJ, Piotrowicz JM. 1984a. Hurricane structure and evolution

as simulated by an axisymmetric nonhydrostatic numerical model. *J. Atmos. Sci.* 41:1169–86

Willoughby HE, Marks FD Jr, Feinberg RJ. 1984b. Stationary and moving convective bands in hurricanes. *J. Atmos. Sci.* 41:3189–211

Withee GW, Johnson A. 1976. *Data report: buoy observations during Hurricane Eloise (September 19 to October 11, 1975)*, US Dep. Commer., NOAA, NSTL Station, MS

Wu C-C, Emanuel KA. 1993. Interaction of a baroclinic vortex with background shear: application to hurricane movement. *J. Atmos. Sci.* 50:62–76

Wu C-C, Emanuel KA. 1995a. Potential vorticity diagnostics of hurricane movement. Part I: a case study of Hurricane Bob (1991). *Mon. Weather Rev.* 122:69–92

Wu C-C, Emanuel KA. 1995b. Potential vorticity diagnostics of hurricane movement. Part II: Tropical Storm Ana (1991) and Hurricane Andrew (1992). *Mon. Weather Rev.* 122:93–109
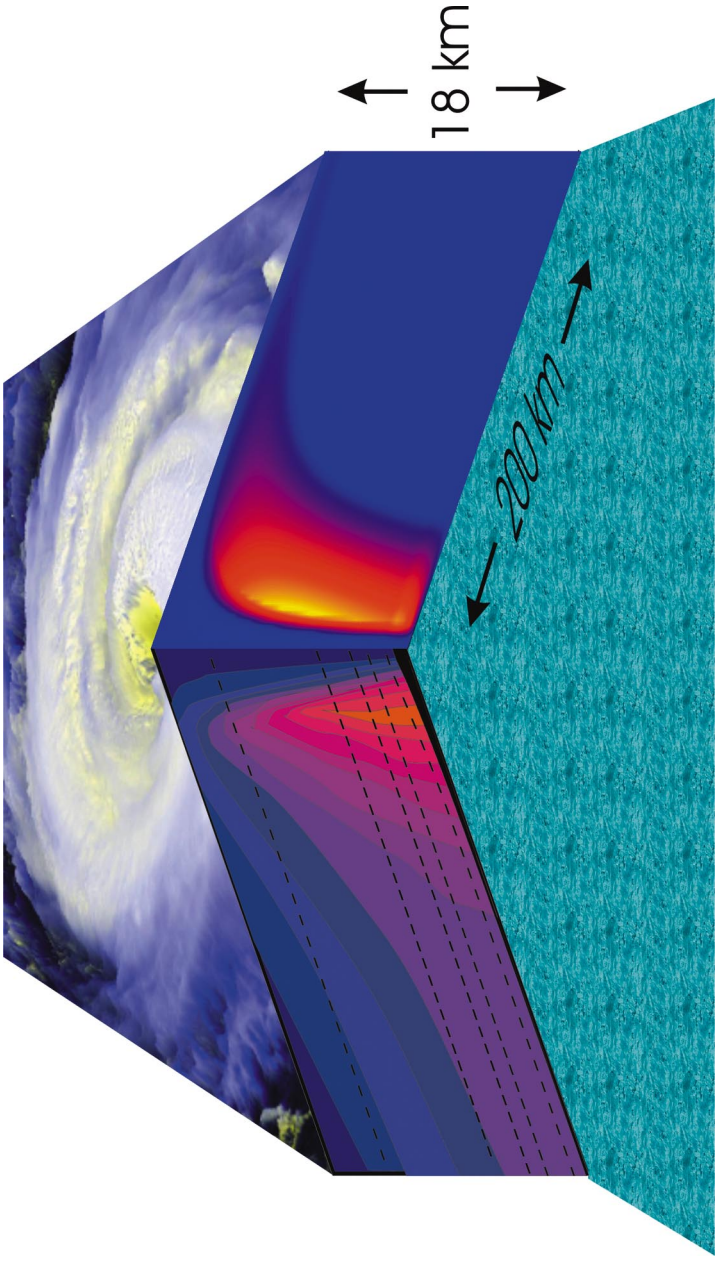
Figure 3 Cutaway view of the structure of a tropical cyclone. The top of the storm is based on a satellite photograph of the cloud structure of Hurricane Fran of 1996. The right-hand cut shows the vertical component of velocity, from a numerical simulation of a hurricane using the model of Emanuel (1995a); maximum values (yellow) are approximately 8 ms^{-1}. The left-hand cut shows the magnitude of the tangential wind component measured in Hurricane Inez of 1966 by aircraft flying at levels indicated by the black dashed lines; from Hawkins & Imbembo (1976). Maximum values are approximately 50 ms^{-1}.
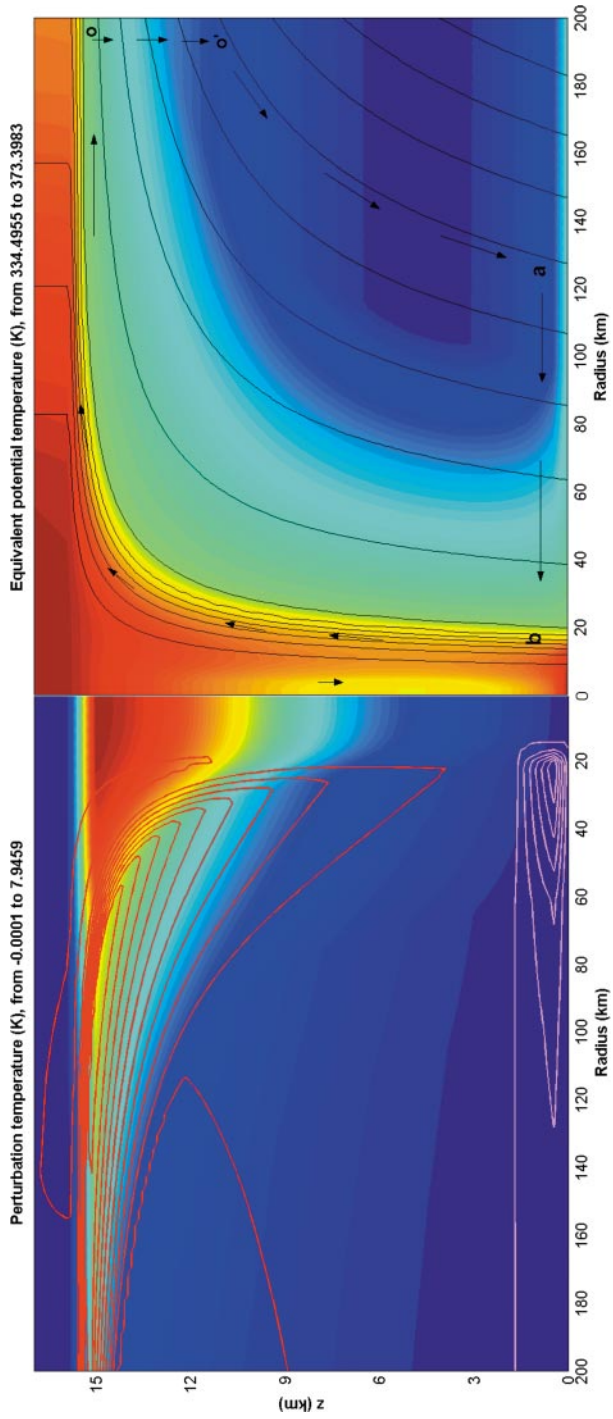
Figure 4 Cross-section of a variety of quantities from a simple numerical model of a tropical cyclone (Emanuel 1995a). The right-hand panel shows a measure of the total specific entropy content of the air (shading), with blue colors denoting relatively small values and red colors showing larger values. The black contours show surfaces of constant absolute angular momentum per unit mass, about the axis of the storm, with values increasing outward. The arrows give an indication of the air motion in this plane. In the left-hand panel, the shading shows the temperature perturbation from the distant environment at the same altitude, with blue colors showing values near zero and red showing high values. The lavender contours near the bottom show the inward radial velocity, whereas the red contours closer to the top show outward radial velocity.